The Astrophysical Journal, 680:580–592, 2008 June 10



# THE EVOLUTION OF THE PECULIAR TYPE Ia SUPERNOVA SN 2005hk OVER 400 DAYS

D. K. Sahu,[1] Masaomi Tanaka,[2] G. C. Anupama,[1] Koji S. Kawabata,[3] Keiichi Maeda,[4,5] Nozomu Tominaga,[2] Ken'ichi Nomoto,[2,5,6] Paolo A. Mazzali,[4,6,7,8] and T. P. Prabhu[1]

*Received 2007 October 12; accepted 2008 February 19*

## ABSTRACT

*UBVRI* photometry and medium-resolution optical spectroscopy of the peculiar Type Ia supernova SN 2005hk are presented and analyzed, covering the premaximum phase to around 400 days after explosion. The supernova is found to be underluminous compared to "normal" Type Ia supernovae. The photometric and spectroscopic evolution of SN 2005hk is remarkably similar to the peculiar Type Ia event SN 2002cx. The expansion velocity of the supernova ejecta is found to be lower than normal Type Ia events. The spectra obtained $\gtrsim$200 days since explosion do not show the presence of forbidden [Fe II], [Fe III], and [Co III] lines, but are dominated by narrow, permitted Fe II, NIR Ca II, and Na I lines with P Cygni profiles. The thermonuclear explosion model with Chandrasekhar mass ejecta and a kinetic energy smaller ($E_K = 0.3 \times 10^{51}$ ergs) than that of canonical Type Ia supernovae is found to well explain the observed bolometric light curve. The mass of $^{56}$Ni synthesized in this explosion is 0.18 $M_\odot$. The early spectra are successfully modeled with this less energetic model, with some modifications of the abundance distribution. The late spectrum is explained as a combination of a photospheric component and a nebular component.

*Subject headings:* supernovae: general — supernovae: individual (SN 2005hk)

## 1. INTRODUCTION

An impressive homogeneity in the light curves and peak luminosities make Type Ia supernovae (SNe Ia) good candidates in the determination of the extragalactic distance scale. Although a majority of the observed SNe Ia belong to the "normal" type (Branch et al. 1993), a number of studies indicate significant photometric as well as spectroscopic differences. For example, studies of nearby supernovae by Li et al. (2001) indicate that 64% SNe Ia are normal, while 20% are of the overluminous SN 1991T type and 16% of the underluminous SN 1991bg type. The peak absolute luminosities of SNe Ia are well correlated with their immediate postmaximum decline rate, forming a photometric sequence from the luminous blue events with a relatively slow decline rate to the faster, red, subluminous events (Hamuy et al. 1996a, 1996b; Phillips et al. 1999).

However, there are a few SNe Ia that are known to deviate from this relation, the most notable among them being SN 2002cx. This supernova was found to be underluminous, but had a light curve decline rate $\Delta m_{15}(B) = 1.29$, comparable to normal SNe (Li et al. 2003). The early-phase ($\lesssim$100 days after explosion) spectra indicate line velocities lower by a factor of 2 compared to those of normal SNe Ia (Li et al. 2003; Branch et al. 2004). Furthermore, the late-phase ($\sim$250 days after explosion) spectra are also quite dissimilar compared to normal SNe Ia, and possibly consist of P Cygni profiles (Jha et al. 2006).

Interestingly, SN 2002cx is not a unique event. Jha et al. (2006) and Phillips et al. (2007) have shown that SN 2005hk shows photometric and spectroscopic behavior almost identical to that of SN 2002cx. Further, Jha et al. (2006) have shown that SNe 2003gq and 2005P also show spectra similar to SN 2002cx. Spectropolarimetric observations of SN 2005hk at the early phases by Chornock et al. (2006) indicate low polarization levels, indicating that the peculiarities of SN 2002cx–like SNe do not result from an extreme asphericity. Based on the analyses of the early-phase spectra of SN 2002cx, Branch et al. (2004) suggest that the observed lower line velocities are consistent with the deflagration models of explosion. Jha et al. (2006) report a possible detection of O I lines in the late-phase spectra and suggest large-scale mixing in the central region, which is also consistent with three-dimensional (3D) deflagration models. Phillips et al. (2007) find that, qualitatively, the observed light curves of SN 2005hk are in reasonable agreement with model calculations of a 3D deflagaration model that produces $\sim$0.2 $M_\odot$ of $^{56}$Ni.

Understanding the nature of this class of SNe Ia is thus quite important for the study of homogeneity and heterogeneity of SNe Ia. It may provide a caution for the cosmological use of SNe Ia and a strong constraint to the explosion models.

We present in this paper the photometric and spectroscopic development of SN 2005hk over $\sim$400 days since explosion.

## 2. OBSERVATIONS AND DATA REDUCTION

### 2.1. *Photometry*

Supernova SN 2005hk was observed in *UBVRI* bands with the 2 m Himalayan Chandra Telescope (HCT) of the Indian Astronomical Observatory (IAO), Hanle, India, using the Himalaya Faint Object Spectrograph Camera (HFOSC), equipped with a SITe 2k $\times$ 4k CCD. The central 2k $\times$ 2k pixels were used for imaging, which corresponds to a field of view of $10' \times 10'$ with a scale of $0.296''$ pixel$^{-1}$. The monitoring of the supernova started on 2005 November 5 (JD 2,453,680), $\sim$4 and $\sim$6 days after its discovery by Burket & Li (see Quimby et al. 2005) and Barentine

[1] Indian Institute of Astrophysics, II Block Koramangala, Bangalore 560034, India.
[2] Department of Astronomy, Graduate School of Science, University of Tokyo, Hongo 7-3-1, Bunkyo-ku, Tokyo 113-0033, Japan.
[3] Hiroshima Astrophysical Science Center, Hiroshima University, 1-3-1 Kagamiyama, Higashi-Hiroshima, Hiroshima 739-8526, Japan.
[4] Max-Planck-Institut für Astrophysik, Karl-Schwarzschild-Strasse 1, Postfach 1317, D-85741 Garching, Germany.
[5] Institute for the Physics and Mathematics of the Universe, University of Tokyo, Kashiwa, Chiba 277-8582, Japan.
[6] Research Center for the Early Universe, Graduate School of Science, University of Tokyo, Bunkyo-ku, Tokyo 113-0033, Japan.
[7] INAF–Osservatorio Astronomico di Trieste, via Tiepolo 11, I-34131, Trieste, Italy.
[8] Kavli Institute for Theoretical Physics, University of California, Santa Barbara, CA 93106.

TABLE 1
MAGNITUDES FOR THE SEQUENCE OF SECONDARY STANDARD STARS IN THE FIELD OF SN 2005hk

| ID | *U* | *B* | *V* | *R* | *I* |
|---|---|---|---|---|---|
| 1..... | 15.896 ± 0.020 | 15.425 ± 0.006 | 14.643 ± 0.004 | 14.174 ± 0.012 | 13.777 ± 0.005 |
| 2..... | 17.257 ± 0.025 | 16.859 ± 0.007 | 16.067 ± 0.005 | 15.579 ± 0.010 | 15.149 ± 0.010 |
| 3..... | 19.175 ± 0.035 | 17.696 ± 0.002 | 16.375 ± 0.009 | 15.564 ± 0.007 | 14.886 ± 0.010 |
| 4..... | 16.824 ± 0.025 | 16.954 ± 0.010 | 16.449 ± 0.016 | 16.097 ± 0.016 | 15.750 ± 0.009 |
| 5..... | 17.842 ± 0.027 | 17.645 ± 0.010 | 16.902 ± 0.009 | 16.440 ± 0.018 | 16.003 ± 0.008 |
| 6..... | 17.094 ± 0.022 | 16.870 ± 0.016 | 16.150 ± 0.010 | 15.706 ± 0.017 | 15.275 ± 0.005 |
| 7..... | 17.834 ± 0.032 | 17.213 ± 0.011 | 16.210 ± 0.012 | 15.646 ± 0.022 | 15.108 ± 0.004 |
| 8..... | 19.134 ± 0.040 | 18.194 ± 0.020 | 17.175 ± 0.014 | 16.571 ± 0.013 | 16.055 ± 0.004 |
| 9..... | 16.366 ± 0.024 | 16.470 ± 0.007 | 16.115 ± 0.007 | 15.871 ± 0.012 | 15.623 ± 0.002 |
| 10..... | 19.516 ± 0.042 | 18.162 ± 0.020 | 16.944 ± 0.010 | 16.201 ± 0.021 | 15.553 ± 0.001 |
| 11..... | ... | 18.059 ± 0.008 | ... | 16.782 ± 0.016 | ... |

NOTE.—The stars are identified in Fig. 1.

et al. (2005), and continued until 2006 September 20 (JD 2,453,999). Standard fields PG 0231+051, PG 1047+003, PG 0942−029, and PG 0918+027 (Landolt 1992) were observed on 2005 November 24 and December 28 under photometric conditions and were used to calibrate a sequence of secondary standards in the supernova field.

The data reduction was done in the standard manner, using various tasks available within IRAF. The observed data were bias-subtracted and flat-field corrected, and cosmic-ray hits were removed. Aperture photometry was performed on the standard stars, using an aperture radius determined on the basis of the aperture growth curve, and were calibrated using the average color terms and photometric zero points determined on the individual nights. The *UBVRI* magnitudes of the secondary standards in the supernova field, calibrated and averaged over the two nights, are listed in Table 1. The secondary sequence is shown marked in Figure 1. The magnitudes of the supernova and the local standards were estimated using the profile-fitting technique, with a fitting radius equal to the FWHM of the stellar profile. The difference between the aperture and profile-fitting magnitude was obtained using bright standards in the supernova field, and this correction was applied to the supernova magnitude. The calibration of the supernova magnitude to the standard system was done differentially with respect to the local standards.

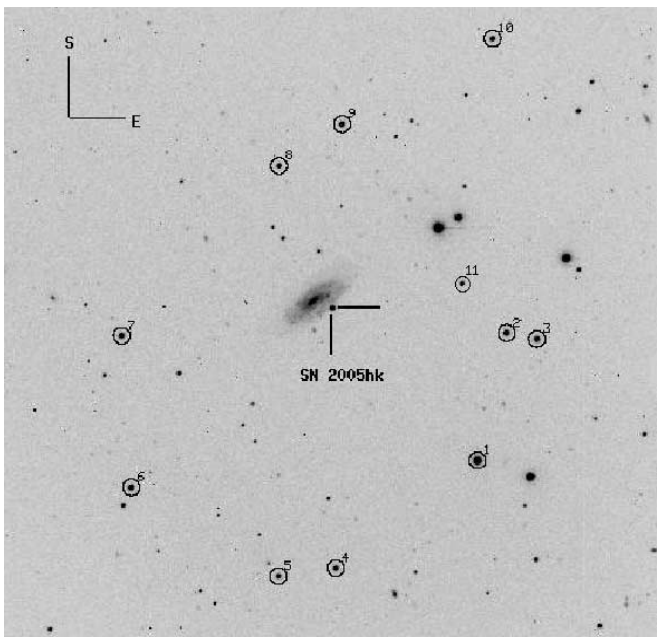


FIG. 1.—Identification chart for SN 2005hk. The stars used as local standards are marked as numbers 1–11.

SN 2005hk was also observed on 2005 December 26, 2006 June 30, and 2006 November 27 with the Faint Object Camera and Spectrograph (FOCAS; Kashikawa et al. 2002), mounted on the 8.2 m Subaru Telescope, in the *B* and *R* bands. The local standard star 11 was calibrated as indicated in Table 1 using the HCT HFOSC photometry of star 2 in Figure 1; then the *B* and *R* magnitudes were derived by the point-spread photometry in the DAOPHOT package of IRAF. The observed supernova magnitudes are listed in Table 2.

### 2.2. *Spectroscopy*

Spectroscopic monitoring of the supernova using the HCT began on 2005 November 4 and continued until 2006 January 12. The journal of observations is given in Table 3. The HCT spectra cover the wavelength ranges 3500–7000 and 5200–9100 Å at a spectral resolution of ∼7 Å. The data reduction was carried out in the standard manner using the tasks available within IRAF. The data were bias-corrected, flat-fielded, and the one-dimensional spectra extracted using the optimal extraction method. Spectra of FeAr and FeNe lamps were used for wavelength calibration. The instrumental response curves were obtained using spectrophotometric standards observed on the same night and the supernova spectra were brought to a relative flux scale. The flux-calibrated spectra in the two regions were combined to a weighted mean to give the final spectrum on a relative flux scale. The spectra were brought to an absolute flux scale using zero points derived by comparing the observed flux in the spectra with the flux estimated using the photometric magnitudes.

Spectra during the late phases were obtained with the Subaru FOCAS on 2005 December 26 and 2006 June 30 and November 27. A 0.8″ wide slit was used with the B300 grism, which gave a wavelength coverage of 4700–9000 Å and a spectral resolution of 11 Å. The exposure times were 900, 1800, and 3600 s for 2005 December 26, 2006 June 30, and 2006 November 27, respectively. The instrumental response was corrected using data from a spectrophotometric standard star (GD 153 or BD +28 4211). The flux was then scaled to be consistent with the *R*-band photometry.

## 3. *UBVRI* LIGHT CURVES

The early-phase light curves (LCs) of SN 2005hk are discussed by Phillips et al. (2007) and Stanishev et al. (2007). Here we present the LCs of this supernova during the early as well as the late phase (Table 2). Figure 2 shows the LCs of SN

TABLE 2
PHOTOMETRIC OBSERVATIONS OF SN 2005hk

| Date | J.D. 2,453,000+ | Phase[a] (days) | $U$ | $B$ | $V$ | $R$ | $I$ |
|---|---|---|---|---|---|---|---|
| 2005 Nov 5..... | 680.06 | −5.22 | ... | 16.126 ± 0.014 | 16.167 ± 0.018 | 16.023 ± 0.014 | 16.060 ± 0.032 |
| 2005 Nov 6..... | 681.04 | −4.25 | 15.482 ± 0.046 | 16.066 ± 0.012 | 16.047 ± 0.011 | 15.934 ± 0.021 | 15.979 ± 0.016 |
| 2005 Nov 7..... | 682.03 | −3.27 | 15.181 ± 0.086 | 16.004 ± 0.046 | 16.007 ± 0.027 | 15.862 ± 0.016 | 15.866 ± 0.039 |
| 2005 Nov 8..... | 683.06 | −2.25 | 15.515 ± 0.060 | 15.966 ± 0.018 | 15.900 ± 0.018 | 15.784 ± 0.013 | 15.798 ± 0.024 |
| 2005 Nov 13..... | 688.04 | 2.66 | 15.741 ± 0.119 | 16.022 ± 0.069 | 15.739 ± 0.050 | 15.631 ± 0.034 | 15.577 ± 0.051 |
| 2005 Nov 15..... | 690.13 | 4.73 | 15.956 ± 0.066 | 16.208 ± 0.027 | 15.710 ± 0.024 | 15.564 ± 0.017 | 15.523 ± 0.016 |
| 2005 Nov 16..... | 691.20 | 5.79 | 16.030 ± 0.058 | 16.260 ± 0.021 | 15.763 ± 0.023 | 15.563 ± 0.016 | 15.416 ± 0.018 |
| 2005 Nov 17..... | 692.14 | 6.72 | 16.222 ± 0.062 | 16.413 ± 0.020 | 15.779 ± 0.020 | 15.568 ± 0.019 | 15.466 ± 0.027 |
| 2005 Nov 19..... | 694.13 | 8.69 | 16.572 ± 0.116 | 16.671 ± 0.021 | 15.840 ± 0.013 | 15.553 ± 0.011 | 15.427 ± 0.025 |
| 2005 Nov 22..... | 697.06 | 11.58 | 17.212 ± 0.037 | 17.132 ± 0.012 | 16.019 ± 0.008 | 15.649 ± 0.015 | 15.466 ± 0.015 |
| 2005 Dec 1 ..... | 706.06 | 20.48 | 18.620 ± 0.021 | 18.260 ± 0.021 | 16.704 ± 0.009 | 16.126 ± 0.015 | 15.796 ± 0.019 |
| 2005 Dec 5 ..... | 710.03 | 24.40 | ... | 18.494 ± 0.011 | 16.925 ± 0.011 | 16.364 ± 0.013 | 15.970 ± 0.019 |
| 2005 Dec 8 ..... | 713.02 | 27.36 | ... | 18.600 ± 0.019 | 17.076 ± 0.010 | 16.501 ± 0.017 | 16.106 ± 0.009 |
| 2005 Dec 12 ..... | 717.03 | 31.32 | ... | 18.758 ± 0.033 | 17.237 ± 0.024 | 16.646 ± 0.025 | 16.251 ± 0.018 |
| 2005 Dec 17 ..... | 722.06 | 36.29 | ... | 18.832 ± 0.016 | 17.362 ± 0.012 | 16.826 ± 0.013 | ... |
| 2005 Dec 23 ..... | 728.13 | 42.29 | ... | 18.846 ± 0.096 | 17.607 ± 0.051 | 17.053 ± 0.041 | 16.593 ± 0.044 |
| 2005 Dec 26[b]..... | 730.79 | 44.92 | ... | 18.859 ± 0.010 | ... | 17.150 ± 0.017 | ... |
| 2005 Dec 26 ..... | 731.14 | 45.27 | ... | 18.944 ± 0.024 | 17.605 ± 0.010 | 17.101 ± 0.009 | 16.698 ± 0.023 |
| 2005 Dec 28 ..... | 733.07 | 47.17 | ... | 19.017 ± 0.014 | 17.618 ± 0.013 | 17.158 ± 0.008 | 16.749 ± 0.008 |
| 2006 Jan 12..... | 748.06 | 61.99 | ... | 19.204 ± 0.031 | 17.920 ± 0.014 | 17.501 ± 0.011 | 17.142 ± 0.027 |
| 2006 Jan 14..... | 750.05 | 63.96 | ... | 19.325 ± 0.045 | 18.038 ± 0.035 | 17.548 ± 0.027 | 17.203 ± 0.015 |
| 2006 Jun 30[b]..... | 917.04 | 230.03 | ... | 21.578 ± 0.033 | ... | 20.140 ± 0.022 | ... |
| 2006 Jul 4 ..... | 921.40 | 233.31 | ... | ... | 20.940 ± 0.044 | ... | ... |
| 2006 Jul 18 ..... | 935.40 | 247.14 | ... | ... | ... | 20.474 ± 0.036 | ... |
| 2006 Sep 20..... | 999.39 | 310.38 | ... | ... | 22.733 ± 0.168 | 21.633 ± 0.099 | ... |
| 2006 Nov 27..... | 1066.73 | 376.98 | ... | 24.206 ± 0.124 | ... | 21.776 ± 0.036 | ... |

[a] Observed phase with respect to the epoch of maximum in $B$ band (JD 2,453,685.34), corrected for the $(1 + z)$ time-dilation factor using the host galaxy redshift $z = 0.0118$.
[b] Subaru photometric observations.

2005hk in the $U$, $B$, $V$, $R$, and $I$ bands, respectively. The epoch of maximum in each of these bands is estimated by a cubic spline fit to the points around maximum. The supernova reached a maximum in the $B$ band on JD 2,453,685.34 with magnitude of 15.91 ± 0.03. The maximum brightness in the $V$, $R$, and $I$ bands occurred at ∼+4, +6.5, and +8.5 days, relative to the maximum in $B$ band, respectively. The decline rate parameter in the $B$ band estimated using our data is $\Delta m_{15}(B) = 1.68 \pm 0.05$. Our estimates of the dates of maximum and apparent maximum magnitudes and the decline rate parameter are listed in Table 4. These estimates are consistent with the values reported by Phillips et al. (2007) and Stanishev et al. (2007).

TABLE 3
LOG OF SPECTROSCOPIC OBSERVATIONS OF SN 2005hk

| Date | J.D. 2,453,000+ | Phase[a] (days) | Range (Å) | Telescope |
|---|---|---|---|---|
| 2005 Nov 4..... | 679.10 | −6.17 | 3500–7000; 5200–9100 | HCT |
| 2005 Nov 5..... | 680.06 | −5.22 | 3500–7000; 5200–9100 | HCT |
| 2005 Nov 6..... | 681.06 | −4.23 | 3500–7000; 5200–9100 | HCT |
| 2005 Nov 13..... | 688.06 | 2.69 | 3500–7000; 5200–9100 | HCT |
| 2005 Nov 15..... | 690.25 | 4.85 | 3500–7000; 5200–9100 | HCT |
| 2005 Nov 17..... | 692.10 | 6.68 | 3500–7000; 5200–9100 | HCT |
| 2005 Nov 20..... | 695.27 | 9.91 | 3500–7000; 5200–9100 | HCT |
| 2005 Nov 23..... | 698.19 | 12.70 | 3500–7000; 5200–9100 | HCT |
| 2005 Nov 24..... | 699.18 | 13.68 | 3500–7000; 5200–9100 | HCT |
| 2005 Dec 1 ..... | 706.09 | 20.50 | 3500–7000; 5200–9100 | HCT |
| 2005 Dec 5 ..... | 710.08 | 24.45 | 3500–7000; 5200–9100 | HCT |
| 2005 Dec 13 ..... | 718.02 | 32.30 | 3500–7000; 5200–9100 | HCT |
| 2005 Dec 26 ..... | 730.81 | 44.94 | 4000–9000 | Subaru |
| 2006 Jan 12..... | 748.09 | 62.02 | 3500–7000; 5200–9100 | HCT |
| 2006 Jun 30 ..... | 916.5 | 228.46 | 4700–9000 | Subaru |
| 2006 Nov 27..... | 1067.05 | 377.26 | 4700–9000 | Subaru |

[a] Observed phase with respect to the epoch of maximum in $B$ band (JD 2,453,685.34), corrected for the $(1 + z)$ time-dilation factor using the host galaxy redshift $z = 0.0118$.

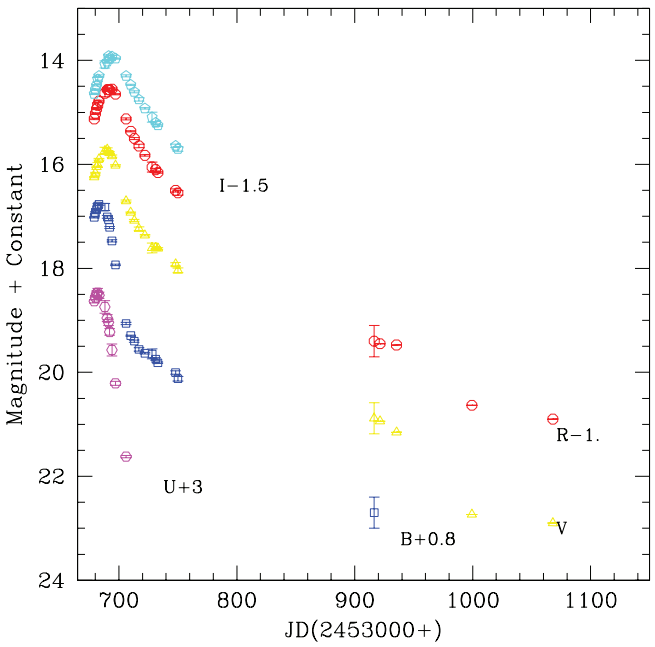


FIG. 2.—*UBVRI* LCs of SN 2005hk. The LCs have been shifted by the amount indicated in the legend.

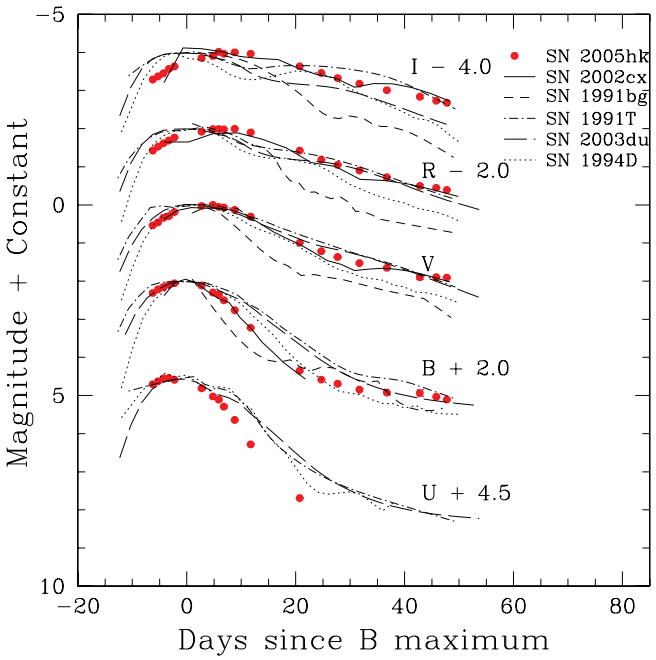


FIG. 3.—Early-phase (<50 days) LC of SN 2005hk together with those of SNe 2002cx, 1991bg, 1991T, 2003du, and 1994D. The ordinate in each panel is the magnitude below the respective maximum, and the abscissae represent the days since respective *B* maximum. For clarity, the LCs have been shifted by the amount indicated in the legend.

The LCs of SN 2005hk are compared with those of the normal SNe 1994D [$\Delta m_{15}(B) = 1.31 \pm 0.08$; Richmond et al. 1995] and 2003du [$\Delta m_{15}(B) = 1.04 \pm 0.04$; Anupama et al. 2005], the overluminous SN 1991T [$\Delta m_{15}(B) = 0.95 \pm 0.05$; Lira et al. 1998], the subluminous SN 1991bg [$\Delta m_{15}(B) = 1.93 \pm 0.08$; Filippenko et al. 1992; Turatto et al. 1996], and the peculiar SN 2002cx [$\Delta m_{15}(B) = 1.29 \pm 0.011$; Li et al. 2003, $\Delta m_{15}(B) = 1.7 \pm 0.1$; Phillips et al. 2007] (Figs. 3–4). The early LCs (Fig. 3) indicate that the premaximum brightening of SN 2005hk was faster than the luminous SN 1991T but comparable to the normal SNe 1994D and 2003du. Following the maximum, during the initial 20 days, the decline in *B* was faster than in normal SNe, but similar to SN 2002cx, while the decline in *V* was similar to the normal SN 1994D. Subsequently, beyond 30 days past maximum, the decline in *B* and *V* was slower than all the other SNe. The secondary peak seen in the *R* and *I* bands of SNe Ia was found to be absent in SN 2005hk, similar to the subluminous SN 1991bg. However, beyond ~50 days past maximum the *R* LC of SN 2005hk had a decline similar to SN 1991T, which is slower than that seen in the normal and subluminous SNe (Fig. 4). The evolution of the *U* light curve of SN 2005hk was found to be faster than both the normal and the luminous types.

The early-phase evolution of SN 2005hk is very similar to that of SN 2002cx. Both objects have similar $\Delta m_{15}(B)$. SN 2005hk has a $\Delta m_{15}(B)$ of 1.68, while SN 2002cx has a value of 1.7, as indicated by the revised photometry by Phillips et al. (2007). On the other hand, at epochs beyond 15 days past maximum, SN 2005hk declines somewhat more slowly than SN 2002cx. The decline rate during ~20–50 days past *B* maximum in the *B*, *V*, *R*, and *I* bands are, respectively, 0.021, 0.027, 0.031, and 0.031 mag day$^{-1}$, while the corresponding decline rates in SN 2002cx during the same phase are 0.037, 0.035, 0.041, and 0.035. It may be noted here that no galaxy template subtraction is done for the data presented here, and the SN magnitudes may be affected by the host galaxy at the later phases. However, as suggested by Phillips et al.

TABLE 4
PHOTOMETRIC PARAMETERS FOR SN 2005hk

| Data | *B* | *V* | *R* | *I* |
|---|---|---|---|---|
| Epoch of maximum[a] | 685.34 ± 0.4 | 689.49 ± 0.8 | 691.78 ± 0.2 | 693.93 ± 0.3 |
| Magnitude at maximum | 15.91 ± 0.03 | 15.71 ± 0.04 | 15.55 ± 0.02 | 15.43 ± 0.03 |
| $\Delta m_{15}(B)$ | 1.68 ± 0.05 | ... | ... | ... |
| Decline rate days 20–45 (mag day$^{-1}$) | 0.021 | 0.027 | 0.031 | 0.031 |
| Decline rate days 230–380 (mag day$^{-1}$) | ... | 0.015 | 0.011 | ... |
| | | COLORS AT *B* MAXIMUM[b] | | |
| | | $B - V$ | $V - R$ | $R - I$ |
| | | −0.03 ± 0.04 | 0.08 ± 0.03 | −0.02 ± 0.06 |

[a] JD 2,453,000+.
[b] Colors are corrected for reddening $E(B - V)_{\rm total} = 0.11$.

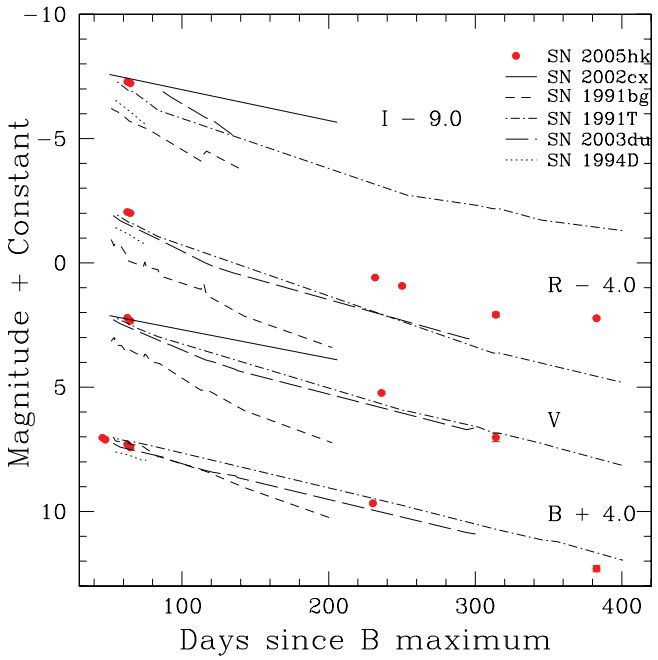


FIG. 4.— Late-phase (>50 days) LC of SN 2005hk together with those of SNe 2002cx, 1991bg, 1991T, 2003du, and 1994D. The ordinate in each panel is the magnitude below the respective maximum, and the abscissae represent the days since respective $B$ maximum. For clarity, the LCs have been shifted by the amount indicated in the legend.

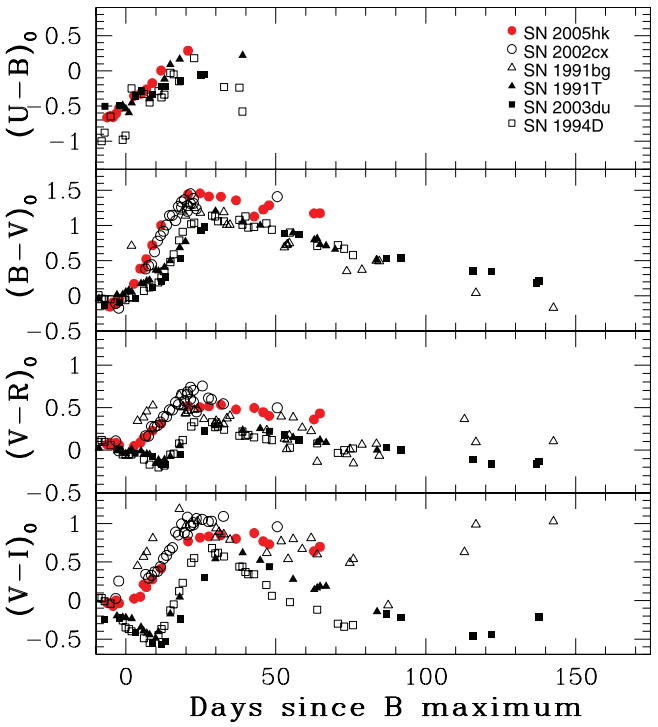


FIG. 5.— $U-B$, $B-V$, $V-R$, and $V-I$ color curves of SN 2005hk. Also shown for comparison are the color curves of SNe 2002cx, 1991T, 1991bg, 2003du, and 1994D. The abscissae correspond to days since respective $B$ maximum.

(2007), neither $K$-correction nor the galaxy background contamination is sufficient to explain the discrepancies seen in the LCs of SN 2005hk and SN 2002cx.

## 4. REDDENING AND COLOR CURVES

The reddening within our Galaxy in the direction of SN 2005hk is $E(B-V)_{\rm Gal} = 0.022$ (Schlegel et al. 1998). The reddening within the host galaxy may be estimated from the methods suggested by Phillips et al. (1999), Altavilla et al. (2004), and Lira (1996). The Phillips et al. (1999) and the Altavilla et al. (2004) methods give $E(B-V)_{\rm Host} = 0.20$ and 0.09, respectively, while the Lira (1996) method indicates a higher value. Spectropolarimetric observations of SN 2005hk (Chornock et al. 2006) indicate an interstellar polarization of 0.27% produced by the host galaxy which, for the standard dust polarization efficiency, corresponds to $E(B-V)_{\rm Host} = 0.09$. Owing to the peculiar nature of SN 2005hk, the methods based on normal SNe Ia may not be applicable. Hence, adopting the estimate for the host galaxy extinction as indicated by the spectropolarimetric observations, we estimate the total reddening toward SN 2005hk to be $E(B-V)_{\rm tot} = 0.11$.

The $U-B$, $B-V$, $V-R$, and $V-I$ color curves of SN 2005hk are shown in Figure 5, compared with other SNe. The color curves of all SNe have been corrected for reddening using the Cardelli et al. (1989) extinction law and the $E(B-V)$ values of $E(B-V) = 0.13$ for SN 1991T (Phillips et al. 1992), $E(B-V) = 0.034$ for SN 2002cx (Li et al. 2003), $E(B-V) = 0.04$ for SN 1994D (Richmond et al. 1995), $E(B-V) = 0.05$ for SN 1991bg (Turatto et al. 1996), and $E(B-V) = 0.01$ for SN 2003du (Anupama et al. 2005).

The color curves of SN 2005hk are very similar to SN 2002cx. The $U-B$ color evolution is very similar to SN 1991T. The $B-V$ and $V-R$ color evolution of SN 2005hk in the premaximum and maximum phase are very similar to the other SNe Ia except SN 1991bg, which had a considerably red color. Beyond $\sim$5 days, until $\sim$20 days after $B$ maximum, both $B-V$ and $V-R$ colors get increasingly redder compared to other SNe, but they remain bluer compared to SN 1991bg. The $V-I$ color, on the other hand, gets redder than other SNe $\sim$5 days before maximum, and it also does not show the dip seen in the color curves of other SNe Ia at $\sim$10 days postmaximum. Beyond $\sim$20 days after maximum, the $V-R$ and $V-I$ colors of SN 2005hk follow the trend of other supernovae and become marginally blue, while $B-V$ continues to be redder than other SNe, including SN 1991bg. Interestingly, despite a very similar color evolution during the premaximum phase to $\sim$20 days after $B$ maximum, SN 2005hk appears to be marginally bluer than SN 2002cx at later phases.

## 5. BOLOMETRIC LIGHT CURVE

### 5.1. *Behavior of Bolometric Light Curve*

The bolometric LC of SN 2005hk is estimated using the *UBVRI* photometry presented here along with the NIR *YJH* photometry reported by Phillips et al. (2007). The magnitudes were reddening-corrected using the value estimated in the previous section and the Cardelli et al. (1989) extinction law. The corrected magnitudes were then converted to monochromatic fluxes using the zero points from Bessell et al. (1998). The bolometric fluxes were derived by fitting a spline curve to the $U$, $B$, $V$, $R$, $I$, $Y$, $J$, and $H$ fluxes and integrating over the wavelength range 3100 Å to 1.63 $\mu$m. In the later phases, when only $B$, $V$, $R$ or $V$, $R$ magnitudes were available, the bolometric flux were estimated by applying a bolometric correction to the available magnitudes. Since SN 2005hk belongs to a rare class of SNe Ia, we derived the bolometric correction from the light curve of SN 2005hk itself, rather than assuming the corrections based on normal SNe Ia (Suntzeff 1996; Contardo et al. 2000). The bolometric corrections were estimated based on the last three points in the LC for which the *BVRIJH* bolometric flux is available. A simple

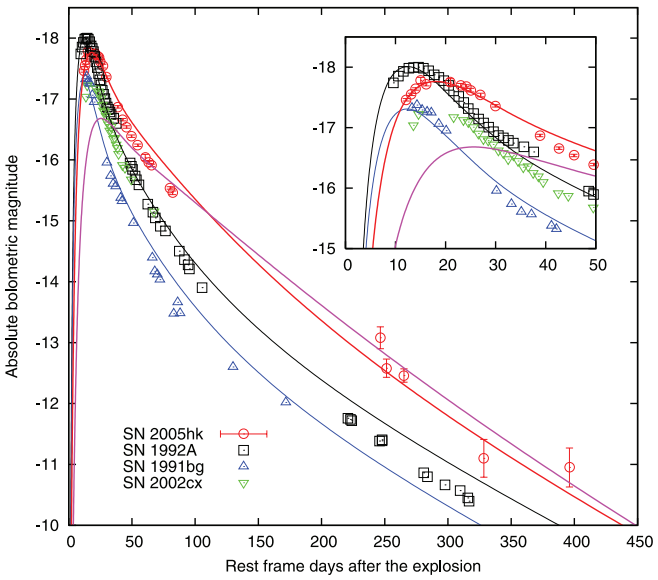


FIG. 6.—Bolometric LC of SN 2005hk (*red circles*) compared with a synthetic LC with the E03 model (*red line*). Black squares and blue triangles are bolometric LCs of SNe 1992A and 1991bg (Suntzeff 1996), respectively. Model LCs for these two SNe are shown in black and blue lines, respectively (based on W7 but different mass of $^{56}$Ni; see Table 5). Green triangles are the bolometric LC of SN 2002cx. In order to fix the rise time of the LCs of SNe 1992A and 1991bg, *B*-band rise time is assumed as $t_{\rm rise} = 19.5 \times s$ days (Conley et al. 2006), where $s$ is stretch factor of *B*-band LC (Goldhaber et al. 2001). The *B*-band rise times of SNe 1992A ($s = 0.80$) and 1991bg ($s = 0.68$) are estimated as 15.6 and 13.2 days, respectively. Since the LC of SN 2005hk is deviated from the normal sequence of SNe Ia, we simply assume $t_{\rm rise} = 17$ days as in Phillips et al. (2007). The magenta line shows the synthetic LC with the E008 model.

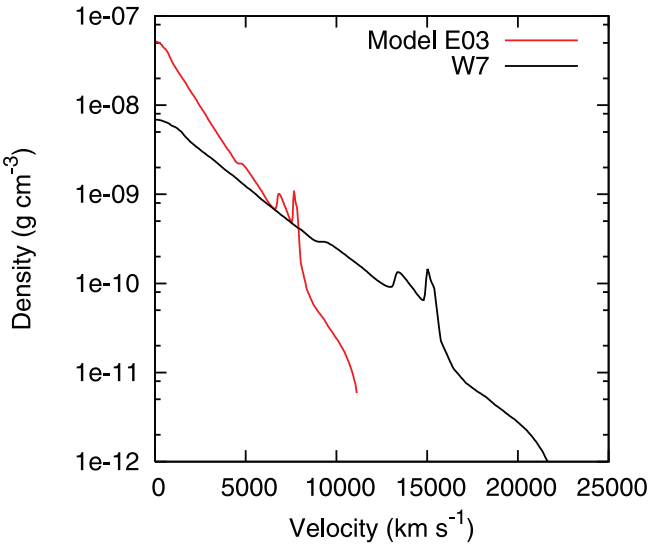


FIG. 7.—Density structure of model E03 compared with that of W7 (1 day after the explosion). The kinetic energy of model E03 is $E_K = 0.3 \times 10^{51}$ ergs. The density structure is scaled from that of W7 homologously. This makes the density at the inner part higher than the original.

average of the bolometric corrections for these days give values of BC $= -0.926 \pm 0.089$ in *B*, BC $= 0.294 \pm 0.045$ in *V*, and BC $= 0.677 \pm 0.027$ in *R* band.

The bolometric LC is plotted in Figure 6 (*red circles*). Also plotted in the figure are the bolometric LCs of the normal (but slightly underluminous) Ia SN 1992A (*black squares*), the subluminous Ia SN 1991bg (*blue triangles*), and SN 2002cx (*green triangles*). The peak luminosity ($M_{\rm bol} = -17.7$) is fainter than the canonical value for normal SNe Ia. It suggests that a smaller amount of $^{56}$Ni is synthesized during the explosion.

The decline of the bolometric LC after the maximum is slower than that of SN 1992A although they have a similar maximum luminosity, as also shown by Phillips et al. (2007). Our observations extend the bolometric LC to ~400 days since explosion. At such late epochs, the bolometric luminosity of SN 2005hk is still brighter than that of SN 1992A. In addition, the difference in the luminosity between the two SNe becomes large, reaching ~1 mag at >250 days after the explosion. The bright late-phase luminosity indicates a more efficient trapping of the $\gamma$-rays from decaying $^{56}$Co in SN 2005hk compared to SN 1992A.

### 5.2. *Light-Curve Modeling*

Phillips et al. (2007) suggest that qualitatively the observed properties of SN 2005hk are consistent with 3D deflagration model (e.g., Röpke et al. 2006; Blinnikov et al. 2006), showing the bolometric and multicolor LC model until ~80 days after the explosion. Branch et al. (2004) and Jha et al. (2006) also suggest a 3D deflagration model for SN 2002cx. Here we give the first investigation of the bolometric LC of this class of SNe until ~400 days after the explosion.

We use an LTE radiation transfer code (Iwamoto et al. 2000) for the computation of the bolometric LCs. For the $\gamma$-ray transport, a gray atmosphere is assumed. For optical radiation transport, electron scattering and line opacity are taken into account. The electron-scattering opacity is evaluated by solving the Saha equation, while the line opacity is crudely assumed to be constant (0.1 cm$^2$ g$^{-1}$; Iwamoto 1997) for simplicity. We use the W7 deflagration model (Nomoto et al. 1984) as a standard density structure and abundance distributions.

First, the mass of $^{56}$Ni [$M(^{56}\mathrm{Ni})$] is varied from the W7 value [$M(^{56}\mathrm{Ni}) = 0.59\,M_\odot$] to obtain a good agreement with the maximum luminosity of SNe Ia shown in Figure 6. In this procedure, the total mass of iron group elements is kept constant to conserve the explosion energy. The black and blue lines in Figure 6 are the synthetic LCs with $M(^{56}\mathrm{Ni}) = 0.17$ and $0.088\,M_\odot$, respectively. Both at the early phase (Fig. 6, *inset*) and the late phase, the LCs are in good agreement with SNe 1992A and 1991bg (Suntzeff 1996), respectively.[9] However, the model sequence with various $M(^{56}\mathrm{Ni})$ never reproduces the brightness of SN 2005hk at $\gtrsim$50 days after the explosion.

As also suggested by Phillips et al. (2007), we now try to explain the LC of SN 2005hk with less energetic models to fit the LC around maximum. We construct a less energetic model simply by scaling the structure of W7 homologously. The mass of the burned material should be adjusted accordingly by taking nuclear energy production into account. In our model, the mass fraction of each burned element is reduced by the same fraction $[(E_K + E_B)/(E_{\rm W7} + E_B)]$ in every radial shell. Here $E_K$, $E_B$, and $E_{\rm W7}$ are the kinetic energy of the SN ejecta, the binding energy of a progenitor WD (~$0.5 \times 10^{51}$ ergs), and the kinetic energy of W7 model (~$1.3 \times 10^{51}$ ergs), respectively. The mass of the burned elements reduced by the procedure above is compensated by unburned C and O, with the mass fraction of $X(\mathrm{C}) = 0.5$ and $X(\mathrm{O}) = 0.5$.

The red line in Figure 6 is the synthetic LC with $M(^{56}\mathrm{Ni}) = 0.18\,M_\odot$ and $E_K = 0.3 \times 10^{51}$ ergs. This kinetic energy is similar to that of the 3D deflagration model used in Phillips et al. (2007). The density structure of this model is given in Figure 7 together with that of the original W7. This model gives a reasonable fit to

[9] This shows that our crude assumption of constant line opacity (0.1 cm$^2$ g$^{-1}$) is reasonable.

TABLE 5
Characteristic Quantities of the Models

| Model (1) | $E_K$ ($10^{51}$ ergs s$^{-1}$) (2) | $M(^{56}\mathrm{Ni})$ ($M_\odot$) (3) | $M(\mathrm{C})$ ($M_\odot$) (4) | $M(\mathrm{O})$ ($M_\odot$) (5) | $M(\mathrm{Si})$ ($M_\odot$) (6) | $M(\mathrm{Fe\ group})$ ($M_\odot$) (7) |
|---|---|---|---|---|---|---|
| W7 (92A)..... | 1.2 | 0.17 | 0.038 | 0.12 | 0.16 | 0.95 |
| W7 (91bg)..... | 1.2 | 0.088 | 0.038 | 0.12 | 0.16 | 0.95 |
| E03 ..... | 0.30 | 0.18 | 0.36 | 0.44 | 0.074 | 0.45 |
| E008 ..... | 0.08 | 0.09 | 0.44 | 0.53 | 0.053 | 0.32 |
| Spectra..... | ... | ... | <0.011 | 0.84 | 0.023 | 0.44 |

Notes.—Col. (2): Kinetic energy of the explosion; col. (3): Total mass of $^{56}$Ni; col. (4): Mass of C contained in the ejecta; col. (5): Mass of O contained in the ejecta; col. (6): Mass of Si contained in the ejecta; col. (7): Total mass of Fe-group elements including $^{56}$Ni.

SN 2005hk at late phase as well as at early phase. In the figure we assume that $B$ maximum of SN 2005hk occurs 17 days after the explosion, which gives the best fit of the LC (see also Phillips et al. 2007).[10] The mass of $^{56}$Ni derived from the model is somewhat smaller than 0.24 $M_\odot$ derived by Phillips et al. (2007). This discrepancy may be caused by a different distribution of $^{56}$Ni in the ejecta. Since $^{56}$Ni in the model in Phillips et al. (2007) is extended to the outer layers, a part of $^{56}$Ni does not contribute to the optical light. In this paper we call our scaled, less energetic model E03.

The behavior of the model E03 LC is understood by simple analysis. If the opacity is assumed to be constant, the timescale of the bolometric LC ($\tau_{\rm LC}$) is scaled as $\tau_{\rm LC} \propto M_{\rm ej}^{3/4} E_K^{-1/4}$ (Arnett 1982), where $M_{\rm ej}$ is the mass of the ejecta. Therefore, if $M_{\rm ej}$ is fixed (Chandrasekhar mass), the lower energy gives a slow decline after the maximum. The late-phase evolution of LC is mainly determined by the optical depth to $\gamma$-rays. Since the optical depth is higher for lower energetic ejecta ($\tau \propto M_{\rm ej}^2 E_K^{-1}$; e.g., Maeda et al. 2003), the LC of model E03 declines slowly at late phase.

The characteristic parameters of the LC models are summarized in Table 5. In the lower energetic model, unburned C and O should be abundant, being $\sim$0.8 $M_\odot$ in total. The presence of large amount of unburned C+O is also seen in 3D deflagration model (Röpke et al. 2006), which is used in Phillips et al. (2007). Although our model is very simple, it mimics the properties of the 3D deflagration model. Our model is further verified by spectral modeling in § 6.3.

## 6. THE SPECTRUM

### 6.1. *Evolution during Early Phases*

The spectral evolution of SN 2005hk during the early phases is shown in Figures 8–12. The premaximum spectra (Fig. 8) show a blue continuum, dominated by Fe III lines, with weak Si II and Ca II H and K absorption (see § 6.3.1). Comparing the premaximum spectrum with other normal Type Ia as well as peculiar Type Ia (Fig. 9), it is seen that the spectrum of SN 2005hk is very similar to that of SN 1991T. However, the minima of the Ca II H and K, Fe II, Fe III, and Si II lines indicate that SN 2005hk has much lower expansion velocities, which decrease from $\sim$6900 km s$^{-1}$ on day $-6$ to $\sim$6200 km s$^{-1}$ on day $-4$. The similarity of the premaximum spectrum of SN 2005hk with SN 1991T–like events has also been noted by Phillips et al. (2007) & Stanishev et al. (2007).

[10] The rise time of 15 $\pm$ 1 days is estimated by Phillips et al. (2007), using 3 $\sigma$ upper limit at 15 days before $B$ maximum. Our model LC assuming the rise time of 17 days is consistent with the upper limit.

The postmaximum evolution of the spectrum of SN 2005hk is presented in Figures 10 and 12. The spectrum and its evolution are quite different from that of normal SNe Ia, as can be seen from Figure 11. The spectrum and its evolution closely matches that of SN 2002cx (Li et al. 2003; Branch et al. 2004; Jha et al. 2006). The spectrum is dominated by Fe II and lines due to Co II, Na I, and Ca II are also clearly present (see § 6.3.1). Some Cr II lines may contribute to the absorption around 4800 Å (Branch et al. 2004). The photospheric velocity decreases to $\sim$4000 km s$^{-1}$ by day +10. The flux in the blue continuum is found to decline steadily, and by day +14, the continuum is quite weak below 4500 Å. This could also be an effect of line blanketing due to Fe II lines. The spectrum remains almost unchanged from day +10 to day +24.

The spectrum of day +62 is very similar to that of day +45, except for the narrowing of lines (Fig. 12). The lines in the 6500–6800 Å, identified with Co II (Branch et al. 2004), which by day +32 started weakening steadily with time (but they could be C II; see § 6.3.1).

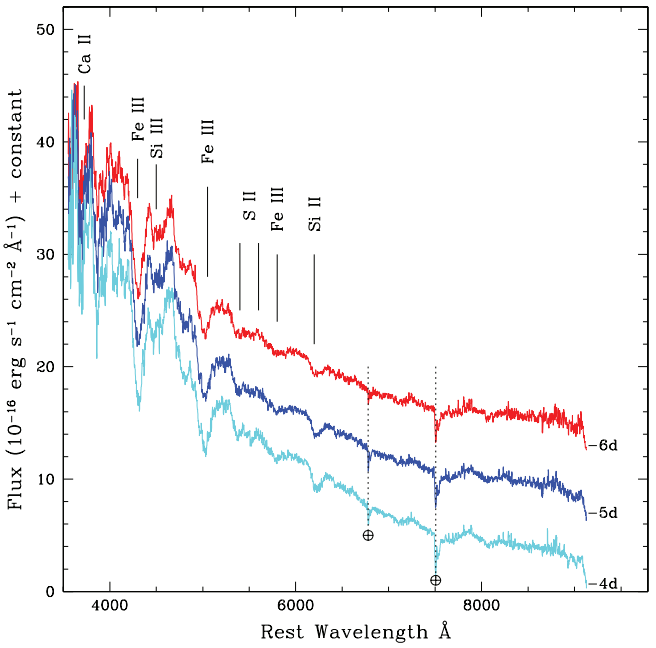


Fig. 8.—Premaximum spectral evolution of SN 2005hk. The phases marked are relative to date of $B$ maximum. The spectra have been corrected for the redshift of the host galaxy, but not corrected for the reddening. For clarity the spectra have been shifted vertically. The telluric lines have not been removed from the spectra and are marked with a circled plus sign.

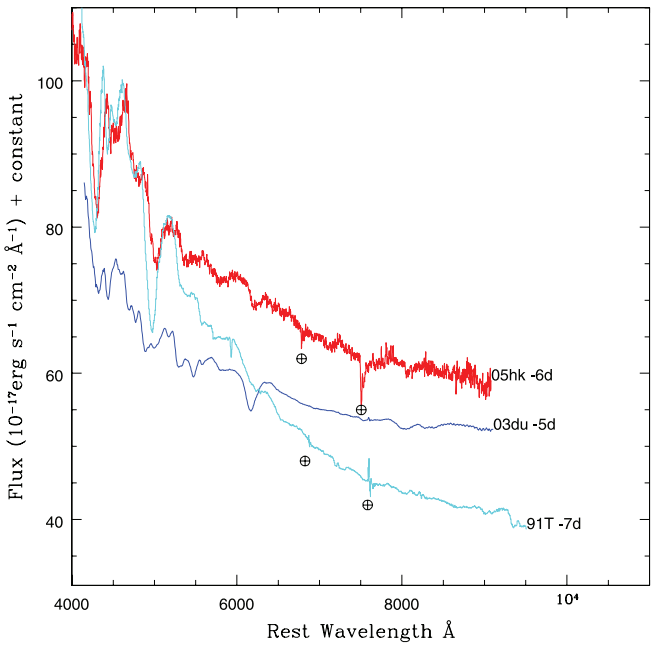


FIG. 9.—Premaximum spectrum of SN 2005hk compared with those of Type Ia SNe 1991T and 2003du at similar epoch. The phases marked are relative to date of *B* maximum. The spectra have been corrected for the redshift of the host galaxy, but not corrected for the reddening. For clarity the spectra have been shifted vertically. The telluric lines have not been removed from the spectra of SNe 2005hk and 1991T, they are marked with a circled plus sign.

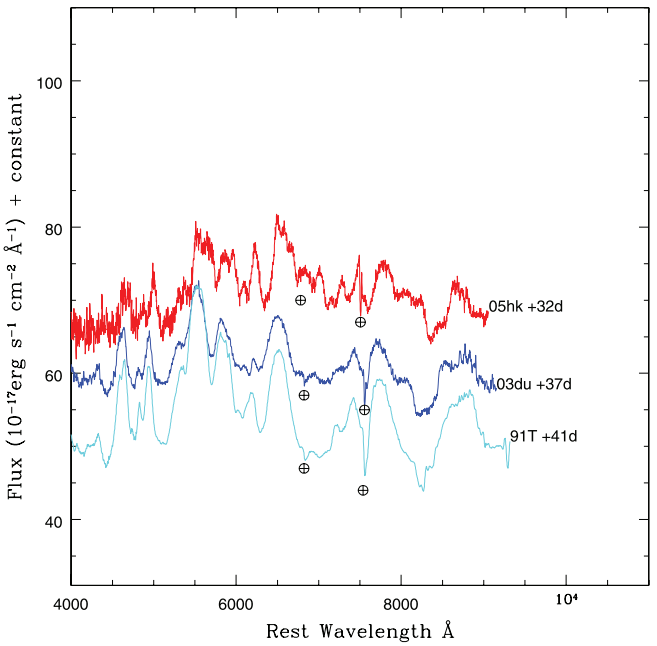


FIG. 11.—Same as Fig. 9, but for the postmaximum spectrum of SN 2005hk compared with those of Type Ia SNe 1991T and 2003du at similar epochs.

### 6.2. *The Late Phases*

The spectra of SN 2005hk were obtained during the late phase on days +228 and +377 (Fig. 13). As in the case of the early-phase spectra, the spectrum of SN 2005hk during these phases is very different from the spectra of normal SNe Ia at similar phases. The spectrum of SN 2005hk is compared with those of other normal and peculiar Type Ia supernovae in Figure 14. The difference between the spectrum of SN 2005hk and spectra of other Type Ia supernovae is obvious. While the other SNe Ia show blends of strong forbidden lines due to iron [Fe II] (5159 Å), [Fe III] (4500–4800 Å), and forbidden lines due to cobalt [Co III] (5890 Å) (Kuchner et al. 1994) in their late-phase spectrum, no signature of these lines is seen in the spectrum of SN 2005hk.

The late-time spectrum of SN 2005hk is dominated by Fe II lines. The Ca II NIR lines are strong and Na I is also present. The spectra of days +228 and +377 (Fig. 13) also show forbidden lines due to [Ca II] $\lambda\lambda$7291, 7234 and [Fe II] at 7155 and 7453 Å.

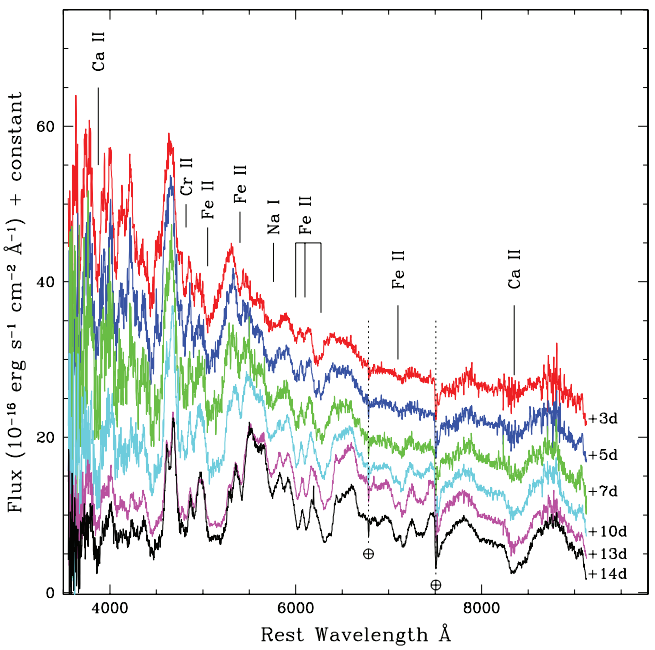


FIG. 10.—Same as Fig. 8, but for the spectral evolution of SN 2005hk from phase +3 days to +14 days relative to date of *B* maximum. Line identification is based on Branch et al. (2004).

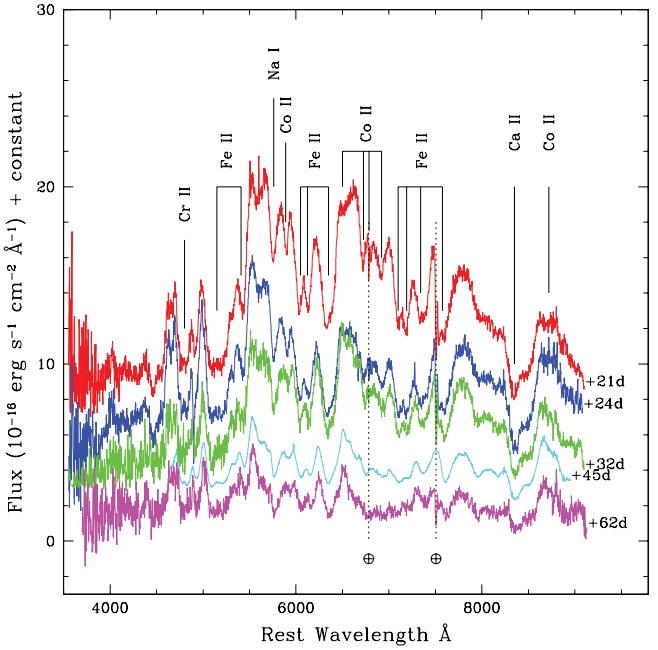


FIG. 12.—Same as Fig. 8, but for the spectral evolution of SN 2005hk from phase +21 days to +62 days relative to date of *B* maximum. Line identification is based on Branch et al. (2004).

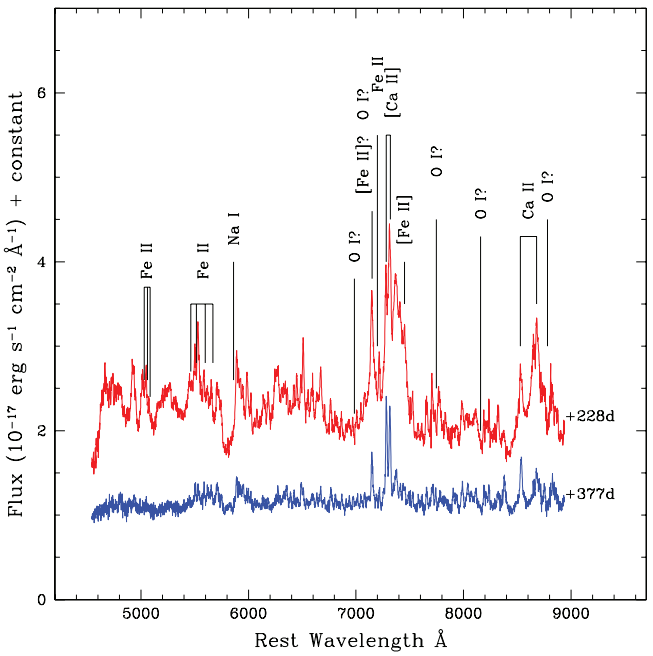


FIG. 13.—Late-phase spectrum of SN 2005hk at +228 days and +377 days relative to date of *B* maximum. The spectra have been corrected for the redshift of the host galaxy, but not corrected for the reddening. For clarity the spectra have been shifted vertically. The telluric lines have been removed from the spectrum. The line identification is based on Jha et al. (2006).

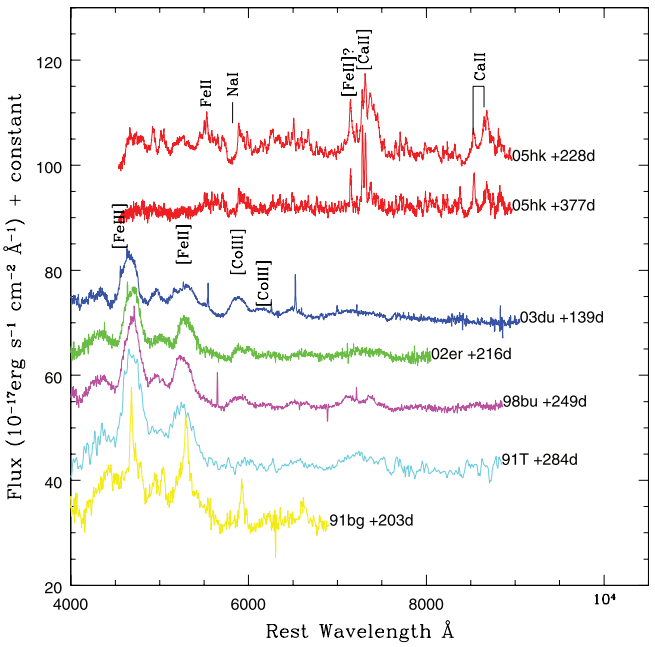


FIG. 14.—Same as Fig. 13, but compared with spectra of other Type Ia SNe: 2003du, 2002er, 1998bu, 1991T, and 1991bg.

The ratio of the fluxes of Ca II NIR and the [Ca II] lines on day +228 indicate densities of $\sim 10^9$ cm$^{-3}$ in the line-emitting region. By day +377, the [Ca II] lines are stronger than the Ca II NIR lines, and the line ratios imply temperatures $\lesssim$4500 K and density $\sim 10^8$ cm$^{-3}$ (Fransson & Chevalier 1989). The mass ejected during the explosion can also be estimated using the number density arrived at with the Ca line ratios. Assuming that the ejecta is moving with a constant velocity of 1000 km s$^{-1}$ over a period of $\sim$380 days after the explosion and a mean atomic weight of $A = 40$, the estimated mass of the ejecta is $\sim 0.25\, M_\odot$. As pointed out by Jha et al. (2006), the mass of the ejecta arrived at is indicative as it does not take into account factors such as clumping or more complicated structures in the line-emitting regions. It may, however, be noted that a high concentration of the mass in the central part is also suggested by the spectral modeling (§ 6.3).

The shift in the central wavelength of the [Ca II] forbidden emission lines indicates an expansion velocity of $\sim$500 km s$^{-1}$ on day +228 and $\sim$300 km s$^{-1}$ on day +377. The FWHM of the emission lines indicate a velocity dispersion of $\sim$1000 km s$^{-1}$ on day +228 and $\sim$500 km s$^{-1}$ on day +377. Similarly, the emission component of the Ca II NIR $\lambda$8542 line indicates an expansion velocity of $\sim$235 km s$^{-1}$ on day +228 and $\sim$210 km s$^{-1}$ on day +377, with velocity dispersions $\sim$2100 and $\sim$1200 km s$^{-1}$, respectively. Low-velocity O I at 7002 and 7773 Å absorption features are clearly identified in the late-phase spectrum. These features were identified, for the first time in any SNe Ia, by Jha et al. (2006) in the "nebular" spectrum of SN 2002cx. The velocity of these lines, measured at the minimum is $\sim$800 km s$^{-1}$. Although there is an overall similarity between the spectra of SN 2002cx and SN 2005hk at late phases, there are some noteworthy differences also. Comparing the spectrum of SN 2005hk on day +228 with the +227 day spectrum of SN 2002cx (Jha et al. 2006), it is found that the expansion velocities and the velocity dispersions are higher in SN 2005hk. The velocity dispersion based on the [Ca II] and the Ca II lines are in fact almost twice that estimated in SN 2002cx.

### 6.3. *Spectral Modeling*

#### 6.3.1. *Early Phases*

The observed spectra of SN 2005hk are further investigated by spectral modeling. For this purpose, we compute synthetic spectra using the Monte Carlo spectrum synthesis code developed by Mazzali & Lucy (1993), Lucy (1999), and Mazzali (2000). We create model spectra at five epochs and compare them with the observed spectra ($-6$, +3, +14, +24, and +45 days from *B* maximum). The rise time is assumed to be 17 days, as in the LC modeling (§ 5.2).

The Monte Carlo spectrum synthesis code assumes a spherical, sharply defined photosphere in the ejecta as an inner boundary. By tracing rays of a number of photon packets emitted from the photosphere, the temperature structure in the SN atmosphere is computed through the flux at each radial point (see eqs. [1] and [2] in Mazzali & Lucy 1993). Radiative equilibrium is assumed for the temperature determination. For the interaction between photons and the SN ejecta, electron scattering and line scattering are taken into account. Sobolev approximation is used for line scattering. Sobolev optical depth is evaluated by computing ionization fractions and electron populations of each ion for a given temperature structure. Details of the physical assumptions adopted in the code are summarized in Mazzali & Lucy (1993), Lucy (1999), and Mazzali (2000).

The input parameters of the code are the position (i.e., velocity, thanks to the homologous expansion) of the photosphere ($v_{\rm ph}$) and the bolometric luminosity ($L$). The parameter $L$ is the emergent luminosity. Since some photons emitted from the photosphere are back-scattered into the photosphere, the luminosity at the photosphere (total photon luminosity emitted from the photosphere) is higher than the input bolometric luminosity $L$ (Mazzali & Lucy 1993). As a density structure we use the less energetic model, which gives the best agreement with the observed LC (model E03; see § 5 and Table 5).

TABLE 6
PARAMETERS OF SPECTRAL FITTING

| Epoch (1) | $v_{ph}$ (km s$^{-1}$) (2) | $M_{r,ph}$ ($M_\odot$) (3) | log ($L$) (4) | $X$(C) (5) | $X$(O) (6) | $X$(Si) (7) | $X$(S) (8) | $X$(Ca) (9) | $X$(Fe) (10) | $X$($^{56}$Ni) (11) |
|---|---|---|---|---|---|---|---|---|---|---|
| −6 ..... | 6500 | 1.11 | 42.56 | <0.001 | 0.86 | 0.002 | 0.021 | 0.001 | 0.020 | 0.035 |
| +3 ..... | 6000 | 1.05 | 42.66 | <0.001 | 0.77 | 0.020 | 0.002 | 0.001 | 0.020 | 0.14 |
| +14 ..... | 3500 | 0.583 | 42.44 | 0.010 (?) | 0.55 | 0.020 | 0.002 | 0.004 | 0.010 | 0.39 |
| +24 ..... | 1500 | 0.128 | 42.19 | 0.010 (?) | 0.53 | 0.020 | 0.022 | 0.004 | 0.40 | |
| +45 ..... | 1000 | $4.90 \times 10^{-2}$ | 41.88 | ... | 0.53 | 0.020 | 0.022 | 0.004 | 0.40 | |
| +228 ..... | 250 | $1.18 \times 10^{-3}$ | 040.86 | ... | 0.53 | 0.020 | 0.022 | 0.004 | 0.40 | |

NOTES.—Col. (1): Days from $B$ maximum; col. (2): Photospheric velocity; col. (3): Mass coordinate at the photosphere; col. (4): Bolometric luminosity (ergs s$^{-1}$) in logarithm; col. (10): Mass fraction of stable Fe; col. (11): Mass fraction of radioactive $^{56}$Ni; The sum of stable Fe and $^{56}$Ni.

The mass fractions of elements are also required for the computation of the synthetic spectra. We treat the mass fractions as parameters rather than using the abundance distribution in the original LC model. The mass fractions of elements are assumed to be homogeneous above the photosphere. We determine the mass fraction of each element to give a good fit of the observed line depths. As time goes by, the photosphere recedes and the absorption lines are formed in the inner part of the ejecta. Nevertheless, we always assume a homogeneous abundance distribution at each epoch, although we change the mass fractions of the elements. The mass fractions derived by the modeling of each spectrum are thought to be a representative abundance ratio near the photosphere because the absorption lines are formed near the photosphere most efficiently.

The parameters in the best-fitting cases are summarized in Table 6. Figure 15 shows the comparison between observed spectra and synthetic spectra. Synthetic spectra are reddened with $E(B-V)_{Gal} = 0.022$ and $E(B-V)_{Host} = 0.09$ (§ 4.). The distance modulus $\mu = 33.46$ is assumed. In the figure the flux and models at each epoch are scaled and shifted for clarity.

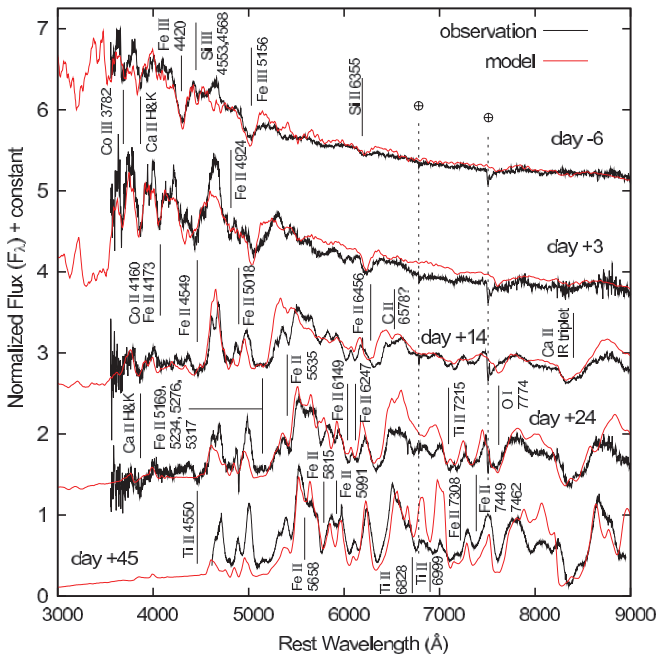


FIG. 15.—Comparison between the observed early-phase spectra of SN 2005hk at (*top to bottom*: −6, +3, +14, +24, and +45 days from $B$ maximum) and the synthetic spectra. Lines that make a major contribution to the absorptions are marked.

The spectrum of SN 2005hk at day −6 is in good agreement with a synthetic spectrum computed with log $L$(ergs s$^{-1}$) = 42.56 and $v_{ph} = 6500$ km s$^{-1}$. The strong absorption features around 4300 and 5000 Å are mainly due to Fe III (Mazzali et al. 1995). The photospheric temperature is computed as $T = 17,000$ K by taking into account the back-scattering effect (Mazzali & Lucy 1993). This high temperature makes the Fe III lines strong and also reproduces the color of the observed spectrum.

The temperature at the photosphere is relatively higher than that of normal Type Ia SNe at similar epoch, and it is comparable to the temperature at very early phase (∼−10 days; Tanaka et al. 2008). The weakness of Si II suggests that the outermost ejecta of SN 2005hk do not contain as much Si [$X$(Si) ∼ 0.02] as is found in normal SNe Ia [$X$(Si) ≳ 0.5]. The S I lines are similarly weak. The mass fraction of S is estimated as $X$(S) ∼ 0.02. The Ca II lines are also very weak, and there is no clear evidence of the high-velocity absorption that is usually seen at premaximum epochs (Mazzali et al. 2005; Tanaka et al. 2006). No C lines are seen, which gives an upper limit of the C mass fraction of $X$(C) ≲ 0.001. The rest of the ejecta consist of oxygen, whose mass fraction is estimated as $X$(O) ∼ 0.86.

The day +3 spectrum matches a synthetic spectrum with log ($L$) (ergs s$^{-1}$) = 42.66 and $v_{ph} = 6000$ km s$^{-1}$. The temperature at the photosphere decreases ($T \sim 9000$ K) from premaximum epochs. The low temperature allows some singly ionized ions such as Si II, Ca II, and Fe II to appear in the spectrum.

The feature at 6300 Å mainly consists of Si II λ6355, and it becomes stronger from premaximum epochs (Figs. 8 and 10). After the maximum, Fe lines begin to contribute to this feature (Figs. 10 and 12). No C lines are visible, giving an upper limit of C mass fraction of $X$(C) ≲ 0.001. The mass fractions of Si, Ca, Fe, and Ni can be estimated by the visible lines (Table 6). The mass fraction of Si, stable Fe, and $^{56}$Ni required for the fitting of this spectrum are larger than those for premaximum spectra. Note again that we assume a spatially homogeneous abundance distribution for each epoch.

After maximum brightness, the evolution of the spectral shape is not significant (Fig. 10). Almost all the absorption features are identified, and they are mostly O I, Ca II, Fe II, and Co II lines. The spectra are reproduced by almost the same element fractions (Table 6). Estimating the mass fraction of stable Fe separately with $^{56}$Ni becomes difficult because more than 25% of $^{56}$Ni, which is one of the dominant elements, has decayed into $^{56}$Fe at ≳40 days after the explosion.

An interesting feature is a weak absorption at 6400 Å in the spectra at day +14 (and possibly in day +24). Branch et al. (2004) suggested that this is a Co II line. However, if we reproduce this feature by Co, the line blocking at ≲4000 Å is too strong, making

the flux there too low. This line could be reproduced by the C II $\lambda$6578 line. This identification is, however, quite marginal. If we assume this feature is the C II, it requires $X(\mathrm{C}) \sim 0.01$. This is larger than the upper limit derived in the preceding spectra, which traces the abundances in the outer layer.

The O I $\lambda$7774 line is always visible in the spectra from day +14 to +45. The O I line is very weak in the earlier spectra, as a result of a severe suppression of the O I fraction due to the high temperature. In fact, the modeling suggests a high O mass fraction in the outermost layers [$X(\mathrm{O}) \gtrsim 0.75$]. These facts clearly indicate that unburned O exists in every place of the ejecta at $v > 1000$ km s$^{-1}$. The mass of O derived from spectral modeling is discussed in § 6.3.2.

### 6.3.2. *Late Phase*

The late-phase spectra of SN 2005hk consist of a combination of P Cygni profiles of permitted lines and emission features of forbidden lines (Fig. 13). We note that no strong [O I] line is seen in the observed spectra. The presence of P Cygni features suggests that the ejecta are not completely transparent even at such late epochs.

We study the late-phase spectra using the model E03, which has similar properties to those of 3D deflagration model. Considering the observed spectra, there seem to be two major problems in this model:

1. The ejecta of the E03 model become optically thin at the late phases. The photospheric velocity becomes zero at 250 days after the explosion if a constant line opacity (0.1 cm$^2$ g$^{-1}$) is assumed.
2. In the E03 model the mass of oxygen is as much as 0.44 $M_\odot$. Such a model would give conspicuous emission lines of [O I] (e.g., Kozma et al. 2005).

First, we create synthetic spectra with the Monte Carlo code used in the modeling of early-phase spectra. Here we assume the presence of the region emitting continuum light at the velocity of $v_{\mathrm{ph}} = 250$ km s$^{-1}$. This could be realized if the central part of the ejecta is denser than that of the E03 model. A synthetic spectrum computed with $\log(L)$ (ergs s$^{-1}$) = 40.86 and with the element mass fraction the same as at day +45 (Fig. 16, *blue line*) is in reasonable agreement with the observed spectrum at day +228, except for emission features at 7300 Å ([Ca II]) and 8600 Å (Ca II). The temperature at the photosphere is as low as 4400 K. Most of the absorption lines are Fe II but some lines of neutral atoms such as Na I and Fe I are also found.

An absorption of the O I $\lambda$7774 line is seen as discussed in § 6.2 (also reported in SN 2002cx; Jha et al. 2006). In the synthetic spectrum, we could get the O I line with the mass fraction $X(\mathrm{O}) \sim 0.5$. Therefore, we conclude that the unburned O is present in whole ejecta, down to very low velocities, suggesting a nearly completely mixed abundance distribution. This property is consistent with 3D deflagration models.

In modeling the early and late-phase spectra, the mass fractions of elements are optimized assuming homogeneous abundance distribution above the photosphere at each epoch. If we assume these mass fractions are characteristic values at each velocity range of the ejecta, the mass of each element can be computed by integrating the density profile of the E03 model. In Table 5 the masses of the C, O, Si, and Fe-group elements derived from spectral modeling are shown. Compared with the masses of the E03 model, a smaller amount of C and Si and larger amount of O are favored in the spectra. The nuclear energy release corresponding to the element abundances obtained from the spectral fitting is $\sim 0.8 \times 10^{51}$ ergs. Since the binding energy of the WD is $\sim 0.5 \times 10^{51}$ ergs, this leads to a kinetic energy of $\sim 0.3 \times 10^{51}$ ergs, which is consistent with the E03 model.

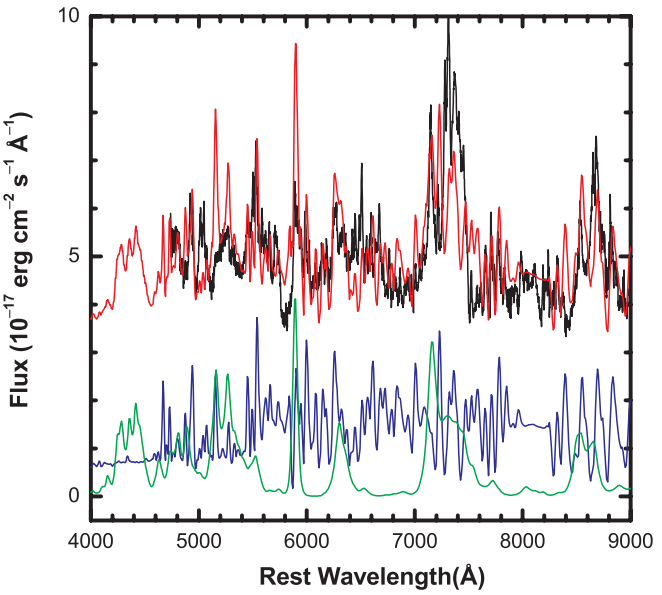


FIG. 16.—Spectrum of SN 2005hk at +228 days with respect to date of $B$ maximum (*black line*; $3 \times 10^{-17}$ ergs cm$^{-2}$ s$^{-1}$ Å$^{-1}$ added to the flux for presentation), as compared to the synthetic "combined" spectrum (*red line*; the same amount added to the flux). The synthetic spectrum is a combination of the photospheric (*blue line*) and the nebular (*green line*) components.

In the computation above, the cooling via lines is not considered, i.e., no emission lines would appear. In order to investigate the emission lines, we compute the late-phase spectra using a nebular synthesis code and consider the combination with the synthetic photospheric spectrum (as in Mazzali et al. 2004).

The nebular code computes the deposition from $\gamma$-rays with a gray opacity (0.025 cm$^2$ g$^{-1}$) using the Monte Carlo method. Positrons are assumed to be trapped in situ. To take into account the different channels in which the deposited energy is consumed, we assume $L_{\mathrm{neb}} = f_{\mathrm{neb}} L_{\gamma,e^+}$, where $L_{\gamma,e^+}$ is the luminosity deposited by the $\gamma$-rays and positrons from 0.18 $M_\odot$ of $^{56}$Co (originally $^{56}$Ni). The fraction, $f_{\mathrm{neb}}$, of $L_{\gamma,e^+}$ is assumed to be balanced by cooling via nebular emission lines, while the other fraction is by photospheric, allowed transitions as modeled by the early-phase spectrum synthesis code. In other words, the luminosity $(1 - f_{\mathrm{neb}})\, L_{\gamma,e^+}$ is deposited below the photosphere, while the remaining luminosity $(f_{\mathrm{neb}}) L_{\gamma,e^+}$ is deposited into the optically thin layer above the photosphere. With this deposition luminosity (with varying $f_{\mathrm{neb}}$), non-LTE rate equations are solved assuming the ionization-recombination equilibrium (Mazzali et al. 2001). Note that the code assumes that the ejecta are optically thin. For the calculation, we assume homogeneous distribution of elements and $^{56}$Co. The masses of these elements are set to be consistent with the E03 model, i.e., $M(^{56}\mathrm{Co}) = 0.18\, M_\odot$ and $M(\mathrm{O}) = 0.4\, M_\odot$.

Figure 16 shows the combination of the photospheric [as described in the first part of this section, with the luminosity corresponding to $M(^{56}\mathrm{Co}) = 0.27\, M_\odot$][11] and nebular components with $f_{\mathrm{neb}} = 0.5$. We find that the [O I] $\lambda\lambda$6300, 6363 doublet is not strong in the model spectra. Indeed, the resulting [O I] is so weak that it is not in contradiction with the nondetection of the [O I], if $f_{\mathrm{neb}} \lesssim 0.5$, as is consistent with the observed, allowed line-dominated spectrum.

[11] This luminosity is higher than that of the E03 model because the late spectrum taken with Subaru is calibrated against the photometry that is brighter than the model LC (Fig. 6) at 250 days after the explosion.

This is an outcome of (1) the high density of the ejecta and (2) the assumption that the elements, especially O and Fe, are homogeneously, thus microscopically, mixed together with one another. With these two conditions, the deposited luminosity is effectively consumed by copious [Fe II] lines rather than [O I].[12] The high density is a direct consequence of the low-energy SN Ia model. However, the complete mixing is a rather extreme assumption, so that we need more detailed modeling of the late-phase spectra of SN 2005hk.

With the nebular component we obtain better fits, compared to purely photospheric component, in the following aspects: (1) strong emission features below ~5500 Å; (2) [Fe II] $\lambda$7155 and [Fe II] $\lambda$7172; (3) [Ca II] $\lambda\lambda$7291, 7324; and (4) Ca II IR and [C I] $\lambda$8727.

The synthetic nebular spectrum for the E03 model results in broader lines than the observed nebular emissions. A typical example is [Ca II] $\lambda\lambda$7291, 7324. The two components are separated in the observations, but blended in the model. This indicates that the nebular line-emitting region is indeed more centrally concentrated than the model. This may again suggest the central part being denser than the E03 model.

In summary, the two major problems numbered 1 and 2 at the beginning of this section could be solved if the ejecta are denser than in the original model and the elements are microscopically mixed. In that case, the ejecta at late phases would consist of three parts: the optically thick innermost part ($v \lesssim 250$ km s$^{-1}$), the optically thin region emitting forbidden lines ($v \lesssim 700$ km s$^{-1}$; i.e., the width of the [Ca II] lines), and the outer layer which is thin even to $\gamma$-rays.

## 7. DISCUSSION

We have studied the bolometric LC and early- and late-phase spectra by computing synthetic LC and spectra. We construct a simple, less energetic model by scaling the kinetic energy of W7 down to $0.3 \times 10^{51}$ ergs. This model (E03) explains the LC of SN 2005hk from early to late phase. The ejecta of the model contain as much as $\sim 0.8\ M_\odot$ of unburned C+O material. In this sense, our less energetic model is similar to the 3D deflagration model.

Branch et al. (2004), Jha et al. (2006), and Phillips et al. (2007) suggested that the properties of SN 2002cx–like objects are similar to those of the 3D deflagration model. We confirm this suggestion by modeling the LC until late phase for the first time. We also find that the early-phase spectra of SN 2005hk are also explained by lower energetic model. The O I absorption is always seen until late phase, suggesting that the elements in the ejecta are mixed almost homogeneously. This is also consistent with the 3D deflagration model.

The late-phase spectra of SN 2005hk do not show strong [O I] line and do show P Cygni profiles of permitted lines. They seem inconsistent with what 3D deflagration model predicts, at a first look. To study this in detail, we modeled the late-phase spectra of SN 2005hk by a combination of the photospheric and nebular components. We find that the innermost region of the ejecta should be denser and more centrally concentrated than that of our model in order to make an optically thick region and a smaller emitting region of nebular lines. The absence of the [O I] line is explained if the elements are microscopically mixed.

In summary, our less energetic explosion model or 3D deflagration model seems to be compatible with the late-phase spectrum of SN 2005hk (and of SN 2002cx–like objects) if (1) the density of the central region is higher than that of our scaled model and (2) the elements are microscopically mixed, although it is a question how such extreme conditions are realized.

The nature of this class of objects can be studied further if observations become available at phases later than those presented here. SN 2005hk is still not completely transparent at ~400 days after the explosion. Only when the ejecta become completely thin can useful information on the structure of the innermost ejecta be obtained.

If there is a subclass of SNe Ia with a lower kinetic energy than in normal SNe Ia, it could present problems for the cosmological use of SNe Ia. To show the effect, we construct a model less energetic than model E03 by scaling the energy of W7 model to $0.08 \times 10^{51}$ ergs ($\sim\frac{1}{4}$ of the kinetic energy of the E03 model). If the deflagration is very weak and slow, such a situation will be realized. Since the nuclear energy release is only slightly higher than the binding energy of the WD, such an explosion could occur after a pulsation (e.g., Nomoto et al. 1976). Since the mass of $^{56}$Ni synthesized by such an explosion is thought to be smaller than that of the E03 model, we set $M(^{56}\mathrm{Ni}) = 0.09\ M_\odot$ ($\frac{1}{2}$ of E03). We call this model E008, and the parameters are summarized in Table 5.

In Figure 6 the synthetic LC with the E008 model is shown as a magenta line. The LC has a fainter peak magnitude than that of the E03 model because of the smaller amount of $^{56}$Ni. However, the decline rate of the LC after maximum is slower than in the E03 model because of the lower kinetic energy of the ejecta. This trend is opposite to the well-known LC-width relation in SNe Ia, i.e., that brighter SNe Ia decline more slowly.

Such explosions can be distinguished by the late-phase LC. Since less energy leads to an efficient trapping of $\gamma$-rays at late phases, the decline rate of the LC at $\gtrsim$100 days after the explosion is slower. This is clearly seen in the synthetic LC (Fig. 6). Although the peak magnitude of the E008 model is fainter than that of the E03 by ~1 mag, the late-phase luminosities of these two models are comparable.

A recently discovered supernova, SN 2007qd, may belong to this subclass (SN 2002cx–like; Bassett et al. 2007; Goobar et al. 2007). This supernova was reported to have reached a fainter maximum than SN 2002cx and SN 2005hk and lower line velocity, being roughly half that of 2002cx or 2005hk. Such properties are realized if the kinetic energy of the ejecta is about quarter that of SN 2002cx (similar to the E008 model), because of the relation of $E_K \propto v^2$. If this is true, the LC of SN 2007qd will evolve very slowly, as shown by the magenta line in Figure 6.

## 8. CONCLUSIONS

Photometric and spectroscopic data on the peculiar SN 2005hk are presented. The *B* band light curve of SN 2005hk shows comparable premaximum brightening—a faster decline in the initial ~20 days past maximum and a slower decline beyond ~50 days past maximum—as compared to normal Type Ia supernovae. The fainter peak bolometric luminosity indicates the synthesis of small amount of $^{56}$Ni in the explosion. The low expansion velocity of the ejecta together with fainter peak luminosity is explained by an explosion with lower kinetic energy. A reasonable fit to the bolometric light curve of SN 2005hk is achieved with a less energetic ($0.30 \times 10^{51}$ ergs) model, which synthesized 0.18 $M_\odot$ of $^{56}$Ni. The light-curve evolution is similar to that of SN 2002cx.

The premaximum spectrum of SN 2005hk is similar to that of SN 1991T, with much lower expansion velocity. The spectral evolution of SN 2005hk is very similar to SN 2002cx. The spectrum of SN 2005hk at late phases (>200 days) is similar to SN 2002cx, except for higher expansion velocities and higher velocity dispersions.

[12] Indeed, [Fe II] around 5200 Å is too strong in the model spectrum, thus smaller value of $f_{\mathrm{neb}}$ is favored.

The presence of P Cygni profiles in the late-phase spectrum of SN 2005hk indicates that the ejecta have not become optically thin up to our final observation. Modeling of the premaximum spectra of SN 2005hk indicates a relatively higher temperature which makes Fe III lines strong. The presence of weak O I line at $\lambda$7774 at almost all epochs is modeled as a consequence of high abundance of completely mixed unburned oxygen in the ejecta. The late-phase spectra of SN 2005hk are modeled as a combination of the photospheric and nebular components, with the nebular line-emitting region being more centrally concentrated than is expected in the case of a less energetic model.

We are thankful to the anonymous referee for valuable comments. This work has been carried out under the INSA (Indian National Science Academy)–JSPS (Japan Society for Promotion of Science) exchange program. This research was supported in part by the National Science Foundation under grant PHY05-51164 and two Grants-in-Aid for Scientific Research (18104003, 18540231) and the 21st Century COE Program (QUEST) of JSPS and MEXT of Japan. M. T. and N. T. are supported through the JSPS Research Fellowships for Young Scientists. K. M. is supported through JSPS Postdoctoral Fellowships for Research Abroad. This work has used data collected at Subaru Telescope, which is operated by the National Astronomical Observatory of Japan. We thank J. Deng for useful discussions and S. Srividya for help in observations and data reduction. We thank all the observers of the 2 m HCT (operated by the Indian Institute of Astrophysics), who kindly provided part of their observing time for the supernova observations. This work has made use of the NASA Astrophysics Data System and the NASA IPAC Extragalactic Database (NED), which is operated by Jet Propulsion Laboratory, California Institute of Technology, under contract with the National Aeronautics and Space Administration.

## REFERENCES

Altavilla, G., et al. 2004, MNRAS, 349, 1344
Anupama, G. C., Sahu, D. K., & Jose, J. 2005, A&A, 429, 667
Arnett, W. D. 1982, ApJ, 253, 785
Barentine, J., et al. 2005, CBET 268
Bassett, B., et al. 2007, CBET 1137
Bessell, M. S., Castelli, F., & Plez, B. 1998, A&A, 333, 231
Blinnikov, S. I., et al. 2006, A&A, 453, 229
Branch, D., Baron, E., Thomas, R. C., Kasen, D., Li, W., & Filippenko, A. V. 2004, PASP, 116, 903
Branch, D., Fisher, A., & Nugent, P. 1993, AJ, 106, 2383
Cardelli, J. A., Clayton, G. C., & Mathis, J. S. 1989, ApJ, 345, 245
Chornock, R., Filippenko, A. V., Branch, D., Foley, R. J., Jha, S., & Li, W. 2006, PASP, 118, 722
Conley, A., et al. 2006, AJ, 132, 1707
Contardo, G., Leibundgut, B., & Vacca, W. D. 2000, A&A, 359, 876
Filippenko, A. V., et al. 1992, AJ, 104, 1543
Fransson, C., & Chevalier, R. A. 1989, ApJ, 343, 323
Goldhaber, G., et al. 2001, ApJ, 558, 359
Goobar, A., et al. 2007, CBET 1137
Hamuy, M., Phillips, M. M., Suntzeff, N. B., Schommer, R. A., Maza, J., & Avils, R. 1996a, AJ, 112, 2391
Hamuy, M., Phillips, M. M., Suntzeff, N. B., Schommer, R. A., Maza, J., Smith, R. C., Lira, P., & Avils, R. 1996b, AJ, 112, 2438
Iwamoto, K. 1997, Ph.D. thesis, Univ. Tokyo
Iwamoto, K., et al. 2000, ApJ, 534, 660
Jha, S., Branch, D., Chornock, R., Foley, R. J., Li, W., Swift, B. J., Casebeer, D., & Filippenko, A. V. 2006, AJ, 132, 189
Kashikawa, N., et al. 2002, PASJ, 54, 819
Kozma, C., Fransson, C., Hillebrandt, W., Travaglio, C., Sollerman, J., Reinecke, M., Röpke, F. K., & Spyromilio, J. 2005, A&A, 437, 983
Kuchner, M. J., Kirshner, R. P., Pinto, P. A., & Leibundgut, B. 1994, ApJ, 426, L89
Landolt, A. U. 1992, AJ, 104, 340
Li, W., Filippenko, A. V., Treffers, R. R., Riess, A. G., Hu, J., & Qiu, Y. 2001, ApJ, 546, 734
Li, W., et al. 2003, PASP, 115, 453
Lira, P. 1996, Master's thesis, Univ. Chile
Lira, P., et al. 1998, AJ, 115, 234
Lucy, L. B. 1999, A&A, 345, 211
Maeda, K., Mazzali, P. A., Deng, J., Nomoto, K., Yoshii, Y., Tomita, H., & Kobayashi, Y. 2003, ApJ, 593, 931
Mazzali, P. A. 2000, A&A, 363, 705
Mazzali, P. A., Danziger, I. J., & Turatto, M. 1995, A&A, 297, 509
Mazzali, P. A., Deng, J., Maeda, K., Nomoto, K., Filippenko, A. V., & Matheson, T. 2004, ApJ, 614, 858
Mazzali, P. A., & Lucy, L. B. 1993, A&A, 279, 447
Mazzali, P. A., Nomoto, K., Maeda, K., & Patat, F. 2001, ApJ, 559, 1047
Mazzali, P. A., et al. 2005, ApJ, 623, L37
Nomoto, K., Sugimoto, D., & Neo, S. 1976, Ap&SS, 39, L37
Nomoto, K., Thielemann, F.-K., & Yokoi, K. 1984, ApJ, 286, 644
Phillips, M. M., Lira, P., Suntzeff, N. B., Schommer, R. A., Hamuy, M., & Jose, M. 1999, AJ, 118, 1766
Phillips, M. M., et al. 1992, AJ, 103, 1632
———. 2007, PASP, 119, 360
Quimby, R., Höflich, P., Kannappan, S. J., Burket, J., & Li, W. 2005, IAU Circ. 8625
Richmond, M. W., et al. 1995, AJ, 109, 2121
Röpke, F. K., Gieseler, M., Reinecke, M., Travaglio, C., & Hillebrandt., W. 2006, A&A, 453, 203
Schlegel, D. J., Finkbeiner, D. P., & Davis, M. 1998, ApJ, 500, 525
Stanishev, V., et al. 2007, in AIP Conf. Ser. 924, The Multicolored Landscape of Compact Objects and Their Explosive Origins, ed. A. Antonelli et al. (Melville, NY: AIP), 336
Suntzeff, N. B. 1996, in Supernovae and Supernova Remnants, ed. R. McCray & Z. Wang (Cambridge: Cambridge Univ. Press), 41
Tanaka, M., Mazzali, P. A., Maeda, K., & Nomoto, K. 2006, ApJ, 645, 470
Tanaka, M., et al. 2008, ApJ, 677, 448
Turatto, M., Benetti, S., Cappellaro, E., Danziger, I. J., della Valle, M., Gouiffes, C., Mazzali, P. A., & Patat, F. 1996, MNRAS, 283, 1